Proceedings of ALGORITMY 2024
pp. 119–128

IMAGE SEGMENTATION OF FLAME FRONT OF A SMOLDERING EXPERIMENT BY GRADIENT FLOW OF CURVES*

MIROSLAV KOLÁŘ†, SHIGETOSHI YAZAKI‡, AND KOYA SAKAKIBARA§

Abstract. In this paper, we review our computational strategy for image segmentation of experimental data of smoldering phenomena by the gradient flow of closed planar curves. The experimental images are preprocessed using an edge-preserving, inhomogeneous Perona-Malik equation. The gradient flow method is modified by a locally acting artificial pushing term penetrating concavities and by tangential redistribution stabilizing the appropriate positioning of discretization points.

Key words. image segmentation, gradient flow, curves, redistribution, Perona-Malik equation

AMS subject classifications. 68U05, 65D18, 14H50, 35R37

1. Introduction.

In the research field of moving boundary problems, many experiments can be regarded as two-dimensional phenomena, such as Hele-Shaw flow, growing snow crystals, annealing of metals, etc.; especially in recent years, an experiment of spreading flame/smoldering fronts along a sheet of paper has been focused on chemical engineering, mathematical modeling, bifurcation theory, data assimilation, and numerical approximation points of view [1, 2, 3, 4, 5]. From any viewpoint, understanding the movement of the moving front in actual experiments is an important task. Hence, this paper presents a novel and simple image segmentation method that can detect expanding smoldering fronts using two-dimensional experimental images. Ultimately, we can detect an expanding smoldering front as a plane polygonal curve. Once we obtain polygonal curves, it is easy to calculate fundamental geometrical quantities such as the curvature, the total length, the enclosed area, the center of gravity, etc.

In digital image processing, identifying the shapes of particular objects of interest is important. Extraction of such shapes for further processing is called segmentation, and today, many different techniques for this problem are available. We can refer the reader to, e.g., statistical methods or graph cut methods [6, 7] and the references therein. In our work, we focus on PDE-based methods for image segmentation.

In this paper, we restrict ourselves to cases of one segmented object whose boundary can be represented by a closed, non-self-intersecting curve in the plane. Such a segmentation curve can be found as a stationary solution of a geometric evolution equation, which can be schematically postulated as

$$\text{normal velocity} = \text{curvature} + \text{force}. \tag{1.1}$$

In (1.1), the curvature term represents the smoothing effect, and the force term pushes the curve toward the boundary of our object of interest. Problem (1.1) can be treated

*This work was supported by JSPS KAKENHI, Grant numbers 21H04593 (SY), 22K03425, 22K18677, and 23H00086 (KS).

† Czech Technical University in Prague, Faculty of Nuclear Sciences and Physical Engineering, Trojanova 13, 120 00, Prague, Czech Republic (Miroslav.Kolar@fjfi.cvut.cz).

‡Graduate School of Science and Technology, Meiji University, 1-1-1 Higashi-Mita, Tama-ku, Kawasaki-shi, Kanagawa 214-8571, Japan (syazaki@meiji.ac.jp).

§ Faculty of Mathematics and Physics, Institute of Science and Engineering, Kanazawa University, Kakuma-machi, Kanazawa-shi, Ishikawa 920-1192, Japan (ksakaki@se.kanazawa-u.ac.jp).

either by implicit tracking methods, such as the level set method or the phase-field method ([8, 9, 10]). However, such methods usually lead to a computationally expensive task with a large number of degrees of freedom. This paper focuses on a direct approach (see [11, 12]) to the problem (1.1), which offers a simple, fast, and straightforward framework for finding a segmentation curve. Such an approach can be easily modified to open curve problems [13, 14] and easily extended to multiple curve problems [15]. It also offers a significant advantage when segmenting a large number of data, typically from a series of images capturing the time evolution of an experiment. An algorithmic approach, as in [16], can be employed for topological changes occurring.

Using the direct approach, we consider a family of closed Jordan curves $\{\Gamma_t \mid t \geq 0\}$ evolving in the plane according to equation (1.1). The curve Γ_t is described by a time-dependent position vector $\boldsymbol{X} = \boldsymbol{X}(t,u)$, where the spatial parameter $u \in [0,1]$. The unit tangent vector $\boldsymbol{T}$ to Γ_t is given as $\boldsymbol{T} = \partial_s \boldsymbol{X}$, where ∂_s is a derivative with respect to arclength s. Here and hereafter, we use $\partial_\xi F = \partial F/\partial \xi$, and $\partial_{\xi\xi} F = \partial_\xi(\partial_\xi F)$. Note that the differential symbol $\mathrm{d}s = |\partial_u \boldsymbol{X}|\,\mathrm{d}u$ and the derivative symbol $\partial_s = |\partial_u \boldsymbol{X}|^{-1}\partial_u$ are both formal abbreviation of RHS, respectively, since the arclength s depends on t and u. The inward unit normal vector to Γ_t is given as $\boldsymbol{N} = \boldsymbol{T}^{\perp}$. From Frenet frame, we can define the curvature κ of Γ_t as $\kappa = \partial_s \boldsymbol{T} \cdot \boldsymbol{N}$. The sign convention of the curvature is such that the curvature of the unit circle is one. Then, the motion of Γ_t can be written as the sum of its normal and tangential part

$$\partial_t \boldsymbol{X} = \beta \boldsymbol{N} + \alpha \boldsymbol{T}, \tag{1.2}$$

where the normal component of the velocity β is given by (1.1), and the tangential part α is briefly discussed in Section 5.

2. Gradient flow method for image segmentation. Gradient flow of evolving closed curves (including various applications) is extensively discussed in, e.g., [17] and references therein. Let us consider a sufficiently smooth inhomogeneous energy density $\gamma(\boldsymbol{x}) > 0$ ($\boldsymbol{x} \in \mathbb{R}^2$) along the curve Γ_t. Then the energy of the curve Γ_t is

$$E(\Gamma_t) = \int_{\Gamma_t} \gamma \,\mathrm{d}s,$$

and its gradient is expressed as

$$-\nabla E = \gamma(\boldsymbol{X})\kappa \boldsymbol{N} - \nabla\gamma(\boldsymbol{X}) \quad \text{on } \Gamma_t. \tag{2.1}$$

The basic idea of image segmentation by gradient flow of curves is described in, e.g., [17]. Let $I(\boldsymbol{x}) \in [0,1]$ be an image intensity function representing a smooth grayscale image, originally scaled from the discrete range $[0,\ldots,255]$, defined on the bounded region (usually it is a rectangle) $\Omega \subset \mathbb{R}^2$.

We define our energy density function as

$$\gamma(\boldsymbol{x}) = \frac{1}{1 + \lambda ||\nabla I(\boldsymbol{x})||^2} \quad \text{for } \boldsymbol{x} \in \Omega. \tag{2.2}$$

Here, such a choice of $\gamma(\boldsymbol{x})$ also represents the edge detector function, where λ is a free parameter of the model. We suggest how to find a suitable parameter λ below. Since the edges in an image are characterized by an abrupt change of the image intensity gradient $||\nabla I(\boldsymbol{x})||$, the value of the edge detector $\gamma(\boldsymbol{x})$ is expected to be low for high

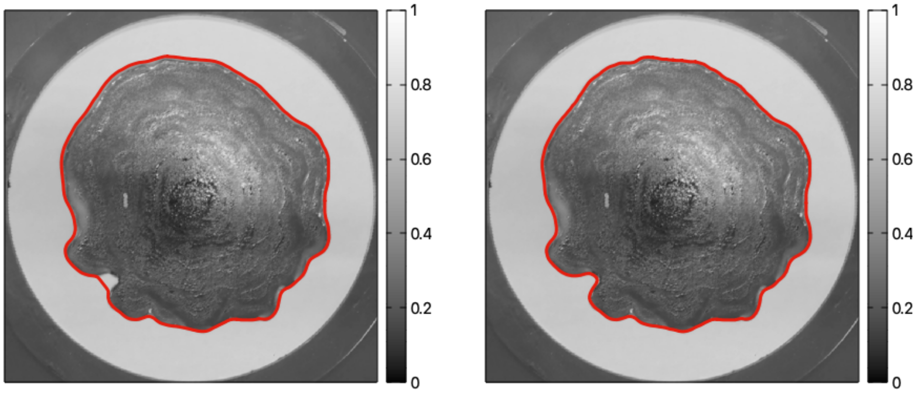

FIG. 2.1. *The effect of artificial pushing force in equation (2.3) to penetrating concavities. In the left figure, no artificial pushing was used. In the right figure, pushing term (2.4) successfully helped the segmentation curve to penetrate through the small hollow in the lower left corner of the smoldered region.*

values of $||\nabla I(\boldsymbol{x})||$ near the edges. Since the flow according to (2.1) minimizes the energy $E(\Gamma_t)$, the curve Γ_t tends to move towards the edges and, upon reaching its local minimum of energy, attain the stationary shape.

Setting $\beta = -\nabla E \cdot \boldsymbol{N}$, the segmentation curve Γ_t is the subject of the following geometric evolution equation

$$\partial_t \boldsymbol{X} = \gamma\kappa - \nabla\gamma \cdot \boldsymbol{N} + \alpha \boldsymbol{T}. \tag{2.3}$$

The gradient flow method approach belongs to the family of *active contour models* (see [12, 18, 19] and references herein). These methods are very sensitive to the choice of the initial segmentation curve Γ_t, and undesirable behavior has been reported. Typically, when the initial segmentation curve Γ_t is chosen far from the segmented object, it can attain a different local minimum of energy, which leads to different stationary solutions. Such unintended behavior is depicted in Fig 2.1.

Our approach to overcome this unintended effect is to add an artificial, locally acting force [14] in the normal direction to Γ_t to equation (2.3), which helps to penetrate concavities or to pass through large segments with almost zero gradient of the image intensity.

We define artificial pushing as the following

$$\mathrm{ap}(\boldsymbol{x}, ||\nabla I(\boldsymbol{x})||) = \begin{cases} \max_{\boldsymbol{x}\in\Omega} ||\nabla I(\boldsymbol{x})|| & \text{if } |\kappa| < \varepsilon \text{ and } ||\nabla I(\boldsymbol{x})|| < \varepsilon \\ 0 & \text{otherwise} \end{cases} \tag{2.4}$$

for $\boldsymbol{x} \in \Omega$. Then, instead of (2.3) we consider the following gradient flow equation

$$\partial_t \boldsymbol{X} = \gamma\kappa - \nabla\gamma \cdot \boldsymbol{N} + \mathrm{ap}\boldsymbol{N} + \alpha \boldsymbol{T}. \tag{2.5}$$

The artificial pushing term $\mathrm{ap} = \mathrm{ap}(\boldsymbol{x}, ||\nabla I(\boldsymbol{x})||)$ in (2.5) is chosen in such a way it moves affected points on the curve Γ_t in the maximal distance of one pixel per the time step during the numerical computations. Let us assume the artificial pushing activates at a particular point on Γ_t, i.e., $|\kappa| < \varepsilon$ and $||\nabla I|| < \varepsilon$. If $I(\boldsymbol{x})$ is $C^2(\Omega)$, then

$||\nabla\gamma|| \le C||\nabla I||$ holds for a constant C depending on λ and the second derivative of I. Therefore if $|\kappa| < \varepsilon$, $||\nabla I(\boldsymbol{X})|| < \varepsilon$, and $\alpha \approx 0$, say $|\alpha| < \varepsilon$, hold on Γ_t, we have

$$||\partial_t \boldsymbol{X}|| \le \varepsilon + C\varepsilon + |\mathrm{ap}| + \varepsilon \lesssim \max_{\boldsymbol{x}\in\Omega} ||\nabla I(\boldsymbol{x})||.$$

After time discretization, we get

$$||\boldsymbol{X}^{n+1} - \boldsymbol{X}^n|| \le \Delta t \max_{\boldsymbol{x}\in\Omega} ||\nabla I(\boldsymbol{x})||.$$

Let us suppose we work with an image of the resolution $M \times M$ pixels, mapped to the square domain $\Omega = (-l/2, l/2) \times (-l/2, l/2)$. The distance between two neighboring points $\boldsymbol{p}_1$ and $\boldsymbol{p}_2$ in an one-pixel is

$$\mathrm{dist}(\boldsymbol{p}_1, \boldsymbol{p}_2) \le \sqrt{2}\frac{l}{M}.$$

Therefore we can estimate the term $\Delta t \max_{\boldsymbol{x}\in\Omega} ||\nabla I(\boldsymbol{x})||$ as the following

$$\Delta t \max_{\boldsymbol{x}\in\Omega} ||\nabla I|| \le \Delta t \max_{\boldsymbol{x}\in\Omega} \sqrt{\partial_x I^2 + \partial_y I^2} \le \Delta t \sqrt{2\left(\frac{1}{l/M}\right)^2} = \Delta t \sqrt{2}\frac{M}{l}.$$

We can estimate the term $\max_{\boldsymbol{x}\in\Omega} ||\nabla I(\boldsymbol{x})||$ as the following

$$\max_{\boldsymbol{x}\in\Omega} ||\nabla I|| \le \max_{\boldsymbol{x}\in\Omega} \sqrt{\partial_x I^2 + \partial_y I^2} \le \sqrt{2\left(\frac{1}{l/M}\right)^2} = \sqrt{2}\frac{M}{l}.$$

Assuming the resolution M is given, we want to discretize our curve by N points to ensure the artificial pushing doesn't move the discretization point more than one-pixel distance per time step, i.e.

$$\Delta t \max_{\boldsymbol{x}\in\Omega} ||\nabla I(\boldsymbol{x})|| \le \Delta t \sqrt{2}\frac{M}{l} \le \sqrt{2}\frac{l}{M}.$$

Therefore, Δt must be chosen in such a way it satisfies the following condition

$$\Delta t \le \frac{l^2}{M^2}. \tag{2.6}$$

3. Treatment of color images. The first problem of color image segmentation is the transformation of the color image, usually stored in RGB or CMY format, into a grayscale image. In industry, the standard for grayscale conversion is the NTSC formula, which transforms the color with (red, green, blue) components into grayscale as the following

$$\mathrm{gray} = 0.299\,\mathrm{red} + 0.587\,\mathrm{green} + 0.114\,\mathrm{blue},$$

where the weighting coefficients are based on the sensitivity of the human eye.

Another way to transform the color image into grayscale is using a color difference function ΔE measured in Lab color space. For our smoldering experimental data, we choose CIE94 standard of the ΔE color difference function [20]. If color differences are calculated correctly, such an approach benefits from emphasizing the segments of the image with bigger perceptual lightness but small differences in color - i.e., the parts close to a flame front.

The process of grayscale transformation is the following. Initially, the source image is converted to the Lab space [21], where RGB components are converted to L*, a*, and b* components denoting lightness, green-red opponents, and blue-yellow opponents, respectively. Then, a reference color is chosen, and for each pixel, we calculate the distance ΔE in Lab space. Finally, these distances are linearized to an 8-bit grayscale image with the pixel intensity within the range $[0, \dots, 255]$ as in [20].

4. Edge preserving smoothing via Perona-Malik equation. Real images always contain various imperfections. The most significant factor for image segmentation is noise, which can prevent the segmentation curve from correctly catching the edges of the desired object. Thus, various preprocessing techniques have been developed to reduce the noise in the image [22, 23, 24]. A typical example of a denoising technique is the artificial image smoothing by heat equation. It can be shown this is equivalent to the convolution of the image intensity function with an appropriate Gaussian kernel. However, such artificial smoothing is homogeneous in all domains, affecting (and destroying) also the edges. Thus, smoothing by heat equation can lead to a loss of information carried by the image.

In our work, we use edge-preserving smoothing by an inhomogeneous diffusion proposed by Perona and Malik [22, 23]. For the image intensity function I, we assume the following Perona-Malik equation

$$\frac{\partial I}{\partial t} = \nabla \cdot (\sigma(||\nabla I||^2)\nabla I), \tag{4.1}$$

where the initial condition $I|_{t=0} = I_0$ is the original image, and the boundary conditions are assumed as, e.g., zero Neumann boundary condition or mirroring. The inhomogeneous function

$$\sigma(s) = \frac{1}{1 + \lambda s}$$

and $||\nabla I(\boldsymbol{x})||^2$ are composed to yield the edge detector function (2.2). Indeed, we have $\sigma(||\nabla I(\boldsymbol{x})||^2) = \gamma(\boldsymbol{x})$. For the numerical discretization, we rewrite equation (4.1) as the following

$$\frac{\partial I}{\partial t} = \nabla\sigma(||\nabla I||^2) \cdot \nabla I + \sigma(||\nabla I||^2)\Delta I, \tag{4.2}$$

which suggests the smoothing effect in (4.1) is locally corrected by the inhomogeneous function σ. In Fig. 3.1, the effect of equation (4.2) is depicted.

For correct behavior of edge-preserving smoothing, choice of free parameter λ in the function $\sigma(s)$ is crucial. Notice $\sigma(0) = 1$ and σ is a decreasing function satisfying $\lim_{s\to+\infty} \sigma(s) = 0$. We define

$$b(s) = \sigma(s) + 2s\sigma'(s) = -2\lambda s\sigma^2(s) + \sigma(s).$$

According to [24], right hand side of Perona-Malik equation (4.1) can be rearranged in terms of σ and b as the following

$$\frac{\partial I}{\partial t} = \sigma(||\nabla I||^2)I_{TT} + b(||\nabla I||^2)I_{NN},$$

where I_{TT} and I_{NN} represent the decomposition of inhomogeneous diffusion terms in tangential and normal directions: $I_{NN} = \partial_N(\partial_N I)$, $\partial_N I = \nabla I \cdot \boldsymbol{N} = -||\nabla I||$ with

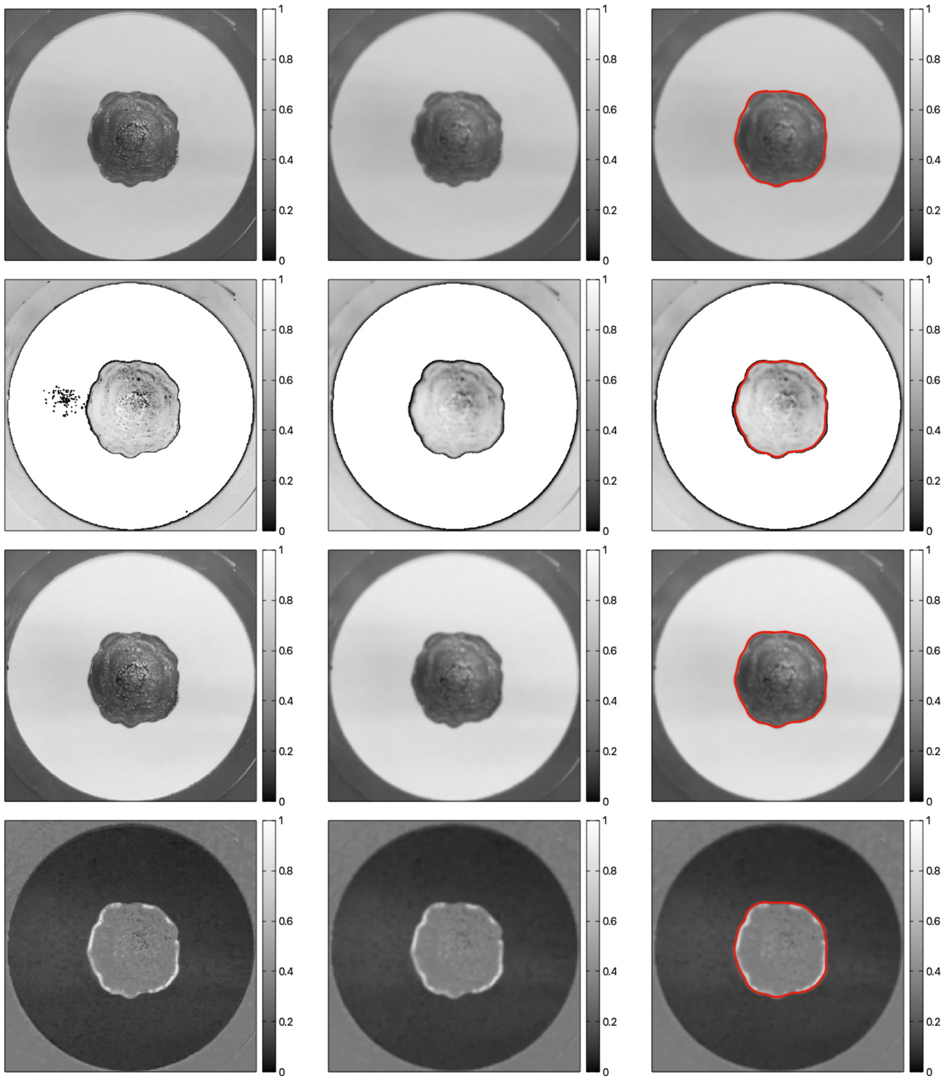

FIG. 3.1. *The comparison of four suitable grayscale candidates for image segmentation.* ***The first column*** *shows the original image transformed into a grayscale. In* ***the second column****, we show the result of artificial smoothing by the Perona-Malik equation (4.2), and finally, in* ***the third column****, the segmentation curve is depicted.*
In ***the first row****, an original image is transformed into a grayscale.* ***The second row*** *depicts differences between the original image and the black color. In* ***the third row****, we show the differences between the original image and the white color. Finally, in* ***the fourth row****, there are differences between the original image and the orange color with RGB coordinates (188,92,68). These coordinates were obtained by averaging of 10 random orange samples of flame front in original RGB image.*
The ***best segmentation results*** *were achieved for the differences between white and orange colors.*

$\boldsymbol{N} = -\nabla I/||\nabla I||$, and then we have $I_{NN} = -\nabla||\nabla I|| \cdot \boldsymbol{N} = ((\mathrm{Hess}\, I)\boldsymbol{N}) \cdot \boldsymbol{N}$ and we define $I_{TT} = \Delta I - I_{NN}$. We require the diffusion in the tangential direction to be dominant, i.e.

$$\lim_{s \to +\infty} \frac{b(s)}{\sigma(s)} = 0.$$

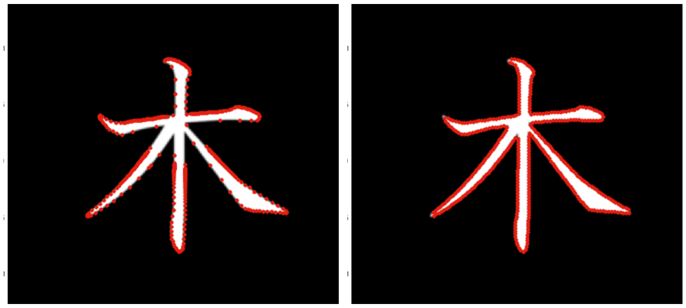

FIG. 5.1. *The effect of tangential redistribution in the binary image of the "ki" character, containing both thin strokes and concavities. The first figure shows the result without the tangential redistribution, which failed to segment the image. In the second figure, we see that asymptotically uniform tangential redistribution (5.1) significantly helps in segmntation.*

This holds if we can force (for large values s (i.e., large values of $||\nabla I||^2$))

$$\frac{s\sigma'}{\sigma} = \frac{-\lambda s\sigma^2}{\sigma} = -\lambda s\sigma = \frac{-\lambda s}{1+\lambda s} \approx -\frac{1}{2},$$

i.e. $\lambda \approx 1/s$. Therefore our choice of λ is

$$\lambda = \frac{1}{\max_{\boldsymbol{x}\in\Omega} ||\nabla I(\boldsymbol{x})||^2}. \tag{4.3}$$

5. The role of tangential velocity functional. It is known that tangential velocity component α in (1.2) does not affect the shape of Γ_t [25]. However, when solving (1.2) numerically, a suitable choice of α is important for the stability of the numerical approximation scheme (see, e.g., Mikula and Ševčovič [11, 12, 17]) and also for the successful attachment of the segmentation curve to the edges in the image. If discretization points along the curve Γ_t are placed nonuniformly, without any possibility of tangential motion, the segmentation procedure could fail in capturing some parts of the image. Such a behavior of curve evolution problem without the tangential velocity is depicted in Fig. 5.1.

Following [12, 17] and denoting the total length of Γ_t as $L(\Gamma_t) = \int_0^1 |\partial_u \boldsymbol{X}(u,t)|\,\mathrm{d}u$, we find the tangential velocity α as the solution of the following problem

$$\partial_s\alpha = \kappa\beta - \langle\kappa\beta\rangle + \left(\frac{L(\Gamma_t)}{|\partial_u \boldsymbol{X}(u,t)|} - 1\right)\omega, \quad \text{where } \langle\kappa\beta\rangle = \frac{1}{L(\Gamma_t)}\int_{\Gamma_t} \kappa\beta\,\mathrm{d}s, \tag{5.1}$$

for $\omega > 0$. It can be shown $\lim_{t\to\infty} \frac{|\partial_u \boldsymbol{X}(u,t)|}{L(\Gamma_t)} = 1$ uniformly with respect to $u \in [0,1]$, which means the discretization points are redistributed asymptotically uniform. Note that α is determined uniquely together with the additional condition $\langle\alpha\rangle = 0$.

6. Strategy to image segmentation. Our objective is to segment the flame front from snapshots of smoldering experiments. Then, we find a time-evolving segmentation curve providing the geometrical information about the flame interface, which can be used to fit the unknown parameters in the flame/smoldering interface model described by the Kuramoto-Sivashinsky model [2, 4]. Assuming we have the time series of images from the experiment, our computational strategy is the following:

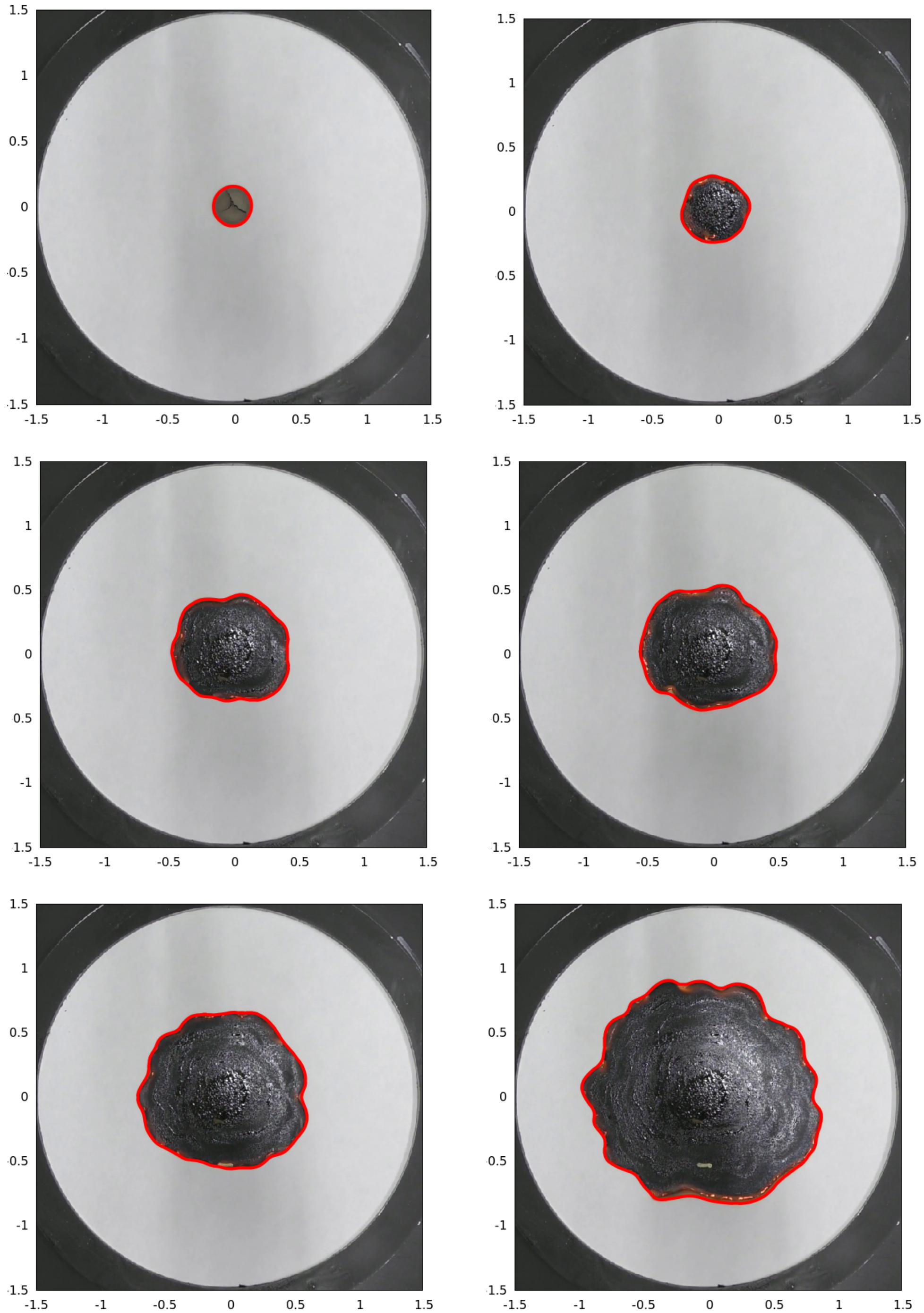

FIG. 5.2. *Successful segmentation of six snapshots of the smoldering experiment. Segmentation curves* Γ_t *were evolved according to equation (2.5) with artificial pushing term (2.4) and asymptotically uniform tangential redistribution (5.1). Segmentation curves* Γ_t *are plotted over original images, which we preprocessed by the Perona-Malik equation (4.2) before the segmentation.*

1. **Initial stage**: choose the appropriate color space for the particular image. Except for RGB and CMY colorspaces, our candidate for suitable colorspace for smoldering experiments is also Lab color space. In Section 3, the transformation from an RGB image to an 8-bit grayscale image of ΔE distances from a reference color (we recommend white or orange) is described.
2. **First stage**: smoothing of the initial image. Initial smoothing and noise reduction can be performed by, e.g., convolution with a Gaussian kernel. We use the edge-preserving smoothing via the Perona-Malik equation (4.2) described in Section 4. Parameter λ in inhomogeneous function $\sigma(s) = 1/(1+\lambda s)$ is chosen as (4.3). Perona-Malik equation (4.2) is discretized by finite differences in space and time integration is done by the explicit Euler method.
3. **Second stage**: evolution of segmentation curve by suitable method. We employ a direct description of the segmentation curve, which is evolved according to the geometrical evolution equation (2.5) given by the gradient flow method described in Section 2. In the edge detector function $\gamma(\boldsymbol{x}) = 1/(1+\lambda||\nabla I(\boldsymbol{x})||^2)$, the free parameter λ is chosen as $\lambda = 0.01$. Moreover, in geometric evolution equation (2.5), the artificial pushing term (2.4) is used to penetrate concavities, and asymptotically uniform tangential redistribution α given by (5.1) is used. The gradient flow equation (2.5) is numerically solved by the flowing finite volumes method described in, e.g., [17]. For stability of artificial pushing, the time step Δt is chosen as in (2.6).
4. **Final stage**: stopping condition. As a stopping criterion for the evolution equation for the segmentation curve, the relative difference in lengths of segmentation curves in time levels n and $n-1$ denoted as L_{t_n} and $L_{t_{n-1}}$, respectively, is used. Calculations stop when

$$\frac{|L_{t_n} - L_{t_{n-1}}|}{L_{t_n}} < \varepsilon,$$

for given $\varepsilon = 10^{-5}$.

7. Conclusions. In this paper, we summarized our computational approach to image segmentation of smoldering experimental data by methods based on PDEs. The consecutive series of experimental images were preprocessed by an edge-preserving, inhomogeneous diffusion equation. We also introduced the optimal choice of the free parameter in the Perona-Malik equation. For the image segmentation, the gradient flow approach was chosen. The known drawback of the gradient flow approach - overcoming concavities - was solved by introducing a novel, locally acting artificial pushing term depending on the curvature of the segmentation curve and the image intensity gradient. We show the stability condition in the sense that the artificial pushing term doesn't move the segmentation curve more than one pixel distance per time step. We successfully applied our computational strategy for segmenting real experimental data and obtained time-evolving geometrical information of the flame front for future processing - see Fig. 5.1. In the upcoming work, we aim to modify the gradient flow approach in the sense of H_1 and segment the experimental data of fingering phenomena.

Acknowledgments. The authors would like to thank Prof. Kazunori Kuwana of Tokyo University of Science for providing us with the experimental data.

REFERENCES

[1] M. Goto, K. Kuwana, G. Kushida and S. Yazaki, *Experimental and theoretical study on near-floor flame spread along a thin solid*, Proceedings of the Combustion Institute, 37 (2019), 3783–3791.
[2] M. Goto, K. Kuwana and S. Yazaki, *A simple and fast numerical method for solving flame/smoldering evolution equations*, JSIAM Lett. 10 (2018), 49–52.
[3] S. Kobayashi and S. Yazaki, *Convergence of a Finite Difference Scheme for a Flame/Smoldering-Front Evolution Equation and Its Application to Wavenumber Selection*, Computational Methods in Applied Mathematics 23 (2022) 545–563.
[4] S. Kobayashi, Y. Uegata and S. Yazaki, *The existence of intrinsic rotating wave solutions of a flame/smoldering-front evolution equation*, JSIAM Lett. 12 (2020) 53–56.
[5] M. Goto, K. Kuwana, Y. Uegata and S. Yazaki, *A method how to determine parameters arising in a smoldering evolution equation by image segmentation for experiment's movies*, Discrete Contin. Dyn. Syst. Ser. S 14 (2019) 881–891.
[6] D. Cremers, M. Rousson, R. Deriche, *A Review of Statistical Approaches to Level Set Segmentation: Integrating Color, Texture, Motion and Shape*, International Journal of Computer Vision, 72 (2007), 195–215.
[7] Y. Boykov, G. Funka-Lea, *Graph cuts and efficient n-d image segmentation*, International Journal of Computer Vision, 70 (2006), 109–131.
[8] A. Handlovičová, K. Mikula and F. Sgallari, *Semi-implicit complementary volume scheme for solving level set like equations in image processing and curve evolution*, Numerische Mathematik, 93 (2003), 675–695.
[9] M. Beneš, V. Chalupecký and K. Mikula, *Geometrical Image Segmentation by the Allen-Cahn Equation*, Applied Numerical Mathematics 51(2) (2013) 187–205.
[10] R. Chabiniok, R. Máca, M. Beneš and J. Tiňtěra, *Segmentation of MRI data by means of nonlinear diffusion*, Kybernetika 49(2) (2013) 301–318.
[11] K. Mikula, D. Ševčovič, *Computational and qualitative aspects of evolution of curves driven by curvature and external force*, Comput. Visual. Sci., 6 (2004), 211–225.
[12] K. Mikula, D. Ševčovič, *Evolution of curves on a surface driven by the geodesic curvature and external force*, Appl. Anal., 85 (2006), 345–362.
[13] M. Kolář, M. Beneš and D. Ševčovič, *Computational analysis of the conserved curvature driven flow for open curves in the plane*, Mathematics and Computers in Simulation, 126 (2016), 1–13.
[14] M. Kolář and S. Yazaki, *Comparison study of image segmentation techniques by curvature-driven flow of graphs*, JSIAM Letters, 13 (2021), 48–51.
[15] M. Beneš, M. Kolář M, and D. Ševčovič , *Curvature driven flow of a family of interacting curves with applications*, Math. Method. Appl. Sci., 43 (2020), pp. 4177-4190.
[16] P. Pauš, M. Beneš, M. Kolář and J. Kratochvíl, *Dynamics of dislocations described as evolving curves interacting with obstacles*, Modelling and Simulation in Materials Science and Engineering, 24 (2016), 035003.
[17] D. Ševčovič and S. Yazaki, *Evolution of plane curves with a curvature adjusted tangential velocity*, Japan J. Indust. Appl. Math., 28 (2011), 413.
[18] Ch. Wai-Pak, L. Kin-Man and S. Wan-Chi, *An adaptive active contour model for highly irregular boundaries*, Pattern Recognition, 34 (2001), 323–331.
[19] V. Srikrishnan, S. Chaudhuri, S. D. Roy and D. Ševčovič, *On Stabilisation of Parametric Active Contours*, in *Computer Vision and Pattern Recognition, IEEE Conference on Computer Vision and Pattern Recognition*, Minneapolis, USA (2007), 1–6.
[20] R. McDonald and K. J. Smith, *Cie94-a new colour difference formula*, Journal of the Society of Dyers and Colourists 111 (1995), 376–379.
[21] I. C. Consortium et al., *Specification icc. 1: 2004-10*, (profile version 4.2.0.0): Image technology colour management (2004).
[22] P. Perona and J. Malik, *Scale-space and edge detection using anisotropic diffusion*, IEEE-Transactions on Pattern Analysis and Machine Intelligence, 12 (1990), pp. 629–639.
[23] F. Catté, P. L. Lions, J. M. Morel and T. Coll, *Image selective smoothing and edge detection by nonlinear diffusion*, SIAM Journal on Numerical Analysis, 29 (1992), pp. 192–193.
[24] G. Aubert and P. Kornprobst, *Mathematical Problems in Image Processing, Partial Differential Equations and the Calculus of Variations*, Springer, New York, 2002.
[25] C. L. Epstein and M. Gage, *The curve shortening flow.* In: A.J. Chorin, A.J. Majda (eds), Wave Motion: Theory, Modelling, and Computation. Mathematical Sciences Research Institute Publications, vol. 7, Springer, New York, 1987.